TECHNICAL UNIVERSITY OF CLUJ-NAPOCA

ACTA TECHNICA NAPOCENSIS

Series: Applied Mathematics, Mechanics, and Engineering
Vol. 67, Issue Special IV, August, 2024

FRACTAL MODELLING OF THE STATIC FRICTION COEFFICIENT IN ELLIPTIC HERTZIAN WHEEL-RAIL CONTACT

Laura Mariana BABICI, Andrei TUDOR, Jordi ROMEU

Abstract: *This research determined that the static friction coefficient uses a fractal approach, which combines the fundamental principles of fractal geometry with the mechanics of contact in both Hertzian wheel-rail systems and the interactions of flat-cylinder specimens that involve rough surfaces. Using the Weierstrass-Mandelbrot model, the study examines the transition through various deformation states, considering the static COF as indicative of the softer material's intrinsic properties and influenced by fractal parameters. Contrasting with the traditional assumption of a homogeneous contact surface, this study integrates fractal properties to calculate the actual contact area more precisely. This approach offers a more nuanced understanding of surface interactions, establishing static COF as a crucial factor for adhesion and a performance indicator in railway operations.*

Key words: *fractal, static friction coefficient, elliptic Hertzian contact, wheel-rail.*

1. INTRODUCTION

Contact mechanics, a key aspect of tribology, examines the stresses and deformations in the contact zones between bodies. Initiated by Hertz in 1882, it has evolved to assess real contact areas in rough surfaces and phenomena like wear and friction. Hertzian contact between wheels and rails is pivotal for efficiency and infrastructure longevity in railway transport. This contact affects wear patterns, noise, and vibrations, involving elastic, elastoplastic, and plastic deformations.

The wheel-rail contact involves interactions between surface asperities, making a real contact area smaller than the apparent one. This necessitates precisely characterising the relationship between this real contact area and the total contact load. Demkin N. B. [1] modelled rough surfaces to analyse contact parameters like actual pressure and friction.

The static friction coefficient (μ_s), crucial for understanding frictional forces, is vital in controlling stick-slip behaviour in railways. Popov V.L [2] and Persson B. N. J., Tossati E. [3] emphasised its role in maintaining adhesion and safety in rail operations.

The actual contact area and surface roughness, central to fields like railway engineering and tribology, significantly influence the static coefficient of friction (μ_s) and slip behaviour.

Greenwood and Williamson's 1966 G.W. model, building on Hertz's elasticity theory, provided a method to determine μ_s, focusing on the elastic deformation of surface asperities, especially under low loads. Chang W. R. et al. [4] later expanded this model for metal joints, considering tangential deformation resistance.

Zhao Y. [5] introduced the ZMC model, incorporating all three deformation stages, diverging from Kogut L. and Etsion I.'s [6] FEM model. This model, aiming to predict static friction in elastoplastic contacts with rough surfaces, emphasised interaction and elastoplastic adhesion. Greenwood J. A. [7] utilised statistical methods, modelling semi-spherical asperities with Gaussian height distributions, highlighting the complexity of modelling random surface roughness.

Two primary approaches are employed in the study of rough surfaces and contact analysis: statistical analysis and fractal theory. Dowson D. [8] discussed that the statistical analysis uses scale-dependent statistical parameters but can yield non-unique results for the same surface. In contrast, fractal theory, highlighted by [9-10], uses scale-independent fractal parameters for a more detailed depiction of roughness.

The CEB model [11] by Chang W. R. et al. [4] and subsequent critiques and advancements by [12-13], emphasise the role of elastoplastic behaviour in contact analysis. This approach challenges the traditional Coulomb friction law by showing that the static friction coefficient (μ_s) decreases with increasing normal load.

Building on fractal theory, researchers like [6], and [14] have developed models to better understand the static friction coefficient for the plane contact surfaces. These models consider variations in fractal parameters, the interaction of roughness elements, and the transition from elastic to plastic deformation. Tian H. et al. [15-16] and Zhang Y. et al. [17] further enhanced this field by developing comprehensive models for understanding contact mechanics and friction dynamics. Using a fractal methodology, our paper investigates the static friction coefficient in rail-wheel Hertzian contact. It leverages the Weierstrass-Mandelbrot model (W-M) to analyse transitions through elastic, elastoplastic, and fully plastic deformation states. The study redefines the static friction coefficient, influenced by fractal parameters D and G_f, as a property of the softer material. It challenges the traditional view of a homogeneous Hertzian contact surface, incorporating fractal properties to accurately calculate the actual contact area. This approach enhances the understanding of surface interactions and the performance of the rail-wheel system, positioning the static friction coefficient as a crucial indicator of adhesion and system efficiency.

2. ANALYSIS OF CONTACT WITH ONE ASPERITY

The mechanical model of a single asperity, depicted using cosine waves, aids in understanding surface roughness and microscopic contact mechanics. This approach is crucial in tribology and Hertzian contact mechanics, especially for examining interactions between rough surfaces like those of wheels and rails. By visualising asperities with varying wave amplitudes and wavelengths, we can better grasp the complexities of Hertzian contact phenomena. Based on the W.M. function, with a wavelength of $l=1/\gamma^n$, (l denotes a general wavelength or a characteristic scale applicable in a broad context, γ is a parameter that defines the frequency density in roughness analysis, and n is the integer number of items gathered by the series during the roughness measurement process), and it indicates the total number of data points considered in the analysis); the shape of individual asperity deformation is described as [18-19]:

$$y(x) = G_f^{(D-1)} l^{2-D} \cos\frac{\pi x}{l},\ -\frac{l}{2} \le x \le \frac{l}{2}. \tag{1}$$

where $y(x)$ represents the height of the roughness profile, D represents the fractal parameter, $(1 < D < 2)$, and G_f is the characteristic scaling length. This interaction can be simplified when the asperities contact, as Figure 1 depicts. In this representation, the contact of the wheel-rail interacting surfaces is condensed to a rail featuring a rough texture. Fractal parameters characterise this textured profile of the surface, as the W-M function outlines.

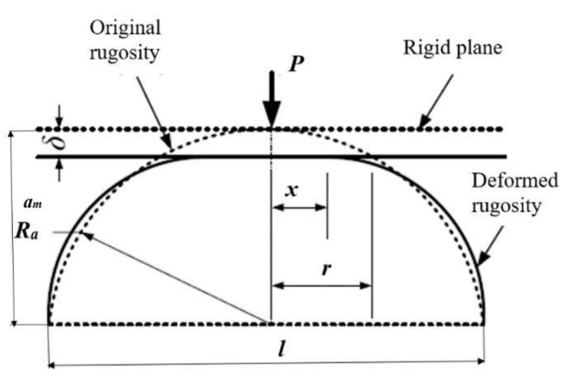

Fig. 1. Schematic model for asperity interaction.

The curvature radius R_a [18] at the peak of the asperity (one cosine) is:

$$R_a = \frac{l^D}{\pi^2 G_f^{(D-1)}}. \tag{2}$$

In this new perspective, l represents the specific base diameter of a fractal asperity at level n within the fractal hierarchy, reflecting the structural characteristic of the asperities at a certain level of fractal detail. This parameter *(l)* is Independent of the deformation δ and spans a range starting from zero up to the maximum amplitude, with $0 \leq \delta \leq a_m$. The deformation (δ) and amplitude (a_m) can be expressed in the following manner [18]:

$$\delta = G_f^{(D-1)} l^{2-D}\left(1-\cos\frac{\pi r}{2l}\right), a_m = G_f^{(D-1)} l^{2-D}. \quad (3)$$

Individual asperity deformation in contact with the rigid plane can be elastic, elastoplastic, or plastic. In the context of Hertzian contact between a wheel and rail, the elastic regime refers to the reversible deformation of surface asperities under load, where materials return to their original shape after the load is removed. This elasticity is crucial for absorbing and distributing stresses, maintaining surface integrity, and ensuring smooth force transmission during wheel-rail interactions, with all deformations being recoverable in the case of single-spot contact.

Based on the Hertz theory [20], the critical deformation (δ_c) caused by an individual asperity, when in contact with a flat, rigid, smooth surface, is:

$$\delta_c = G_f\left(\frac{2E}{k \cdot H_d}\right)^{\frac{2-D}{D-1}}. \quad (4)$$

where, H_d is the hardness of the softer material, k represents the coefficient related to the Poisson ratio of the wheel [4] with k=0.454+0.41ν, and E is the equivalent Hertzian elastic modulus defined as:

$$\frac{1}{E} = \frac{1-\nu_1^2}{E_1} - \frac{1-\nu_2^2}{E_2}. \quad (5)$$

where E_1, E_2 and ν, ν_1, ν_2 are Young's modulus and Poisson's ratios of the wheel and rail materials, respectively, in the case of the rigid flat $E_2 \rightarrow \infty$.

When the deformation δ equals the critical value δ_c, the individual asperity undergoes elastic deformation. Material remains in the elastic regime and returns to its original shape after stress is removed, as long as the deformation is less than a critical value ($\delta < \delta_c$), preventing any permanent or plastic changes. When deformation exceeds a critical value ($\delta > \delta_c$), the material enters the elastoplastic or plastic regime, leading to irreversible changes and preventing it from returning to its original shape, impacting friction and wear in mechanical systems.

2.1 Critical area

Based on the Majumdar Bhushan model (M.B. model) [10], the critical contact area (a_c) concept associated with surface roughness deformation serves as a fundamental boundary that distinguishes between the regimes of elasticity and plasticity in contact mechanics.

Given that the asperity's curvature radius is significantly larger than its amplitude, specifically $R_a >> a_m$ [21-22].

This critical contact area (a_c) and its dimensionless form a_{cs} are expressed as:

$$a_c = G_f^{\,2}\left(\frac{2E}{kH_d}\right)^{2/(D-1)}, \; a_{cs} = \frac{G_{fs}^{\,2}}{\left(k\,\frac{k_{HE}}{2}\right)^{2/(D-1)}},$$

$$k_{HE} = \frac{H_d}{E}. \quad (6)$$

where, the dimensionless form are the expressions:

$$a_{cs} = \frac{a_c}{A_a}, G_{fs} = \frac{G_f}{\sqrt{A_a}}. \quad (7)$$

where A_a represents the nominal or apparent area of wheel-rail surfaces with fractal roughness, which refers to the apparent or macroscopic contact area and is the area one would observe without any magnification, essentially the projected area of one object onto the other, G_{fs} represent G_f dimensionless form, and k_{HE} is the hardness factor. The nominal area for the Hertzian contact depends on the load applied due to elastic deformation, radius curves of rail and wheel, and material properties, which directly influence G_{fs}.

2.2 Contact spot area

The asperity's deformation enters the plastic regime when the contact spot area of surfaces with fractal roughness a (with a_s its dimensionless form) is less than a_{cs}. In contrast, if a_s exceeds a_{cs}, the regime shifts to an elastic state. The dimensionless contact spot area a_s and asperity deformation $\delta_s(a_s)$ have the following equations expressed by fractals:

$$a_s = \frac{a}{A_a}, \quad a_s = G_{fs}^{\frac{2D-2}{D-2}} \delta_s^{\frac{2}{2-D}} . \qquad (8)$$

Subsequently, the dimensionless contact load in the elastic state (P_{se}) may be expressed by fractals depending on the roughness corresponding to the contact dimensionless area a_s as follows:

$$P_{se}(a_s) = \frac{4\sqrt{\pi} G_{fs}^{D-1}}{3} a_s^{(3-D)/2}, P_{se} = \frac{P_e}{A_a E} . \quad (9)$$

where, dimensionless P_{se} denote the contact loads of a distorted asperity in the elastic regime.

2.3 Elastoplastic deformation regime

In the context of Hertzian contact between wheel and rail, the elastoplastic regime is particularly significant as it determines how forces are transmitted and distributed across the contact asperities. This regime indicates the onset of plastic flow and can affect the static and dynamic friction coefficients and the wear of both the wheel and the rail. The critical factor here is the threshold at which the elastic deformation of the asperities transitions into plastic deformation. This is determined by the material properties of the asperities, such as hardness and yield strength. In railway engineering, understanding and managing this deformation regime is vital for optimising wheel-rail contact to minimise wear and maintain traction, which directly contributes to the safety and efficiency of rail transport.

Next, the critical deformations for elastoplastic deformation's first and second stages are evaluated. As per the findings of Kogut (*Kogut L. and Etsion I., 2004*), when expressed dimensionless, the complete elastoplastic regime of a deformed one asperity falls within the range of $1 \le \frac{\delta_s}{\delta_{cs}} \le 110$. Here, δ_s represents the dimensionless asperity deformation, and δ_{cs} represents the dimensionless critical asperity deformation, completely dependent on the material property in which the following equations give δ_s and δ_{cs}:

$$\delta_s(a_s) = G_{fs}^{D-1} a_s^{\frac{2-D}{2}}, \ \delta_{cs} = G_{fs}^{D-1} a_{cs}^{\frac{(2-D)}{2}} . \qquad (10)$$

Furthermore, this entire elastoplastic regime is divided into two distinct phases: the first regime, where deformation values range from $1 \le \frac{\delta_s}{\delta_{cs}} \le 6$, the hemisphere undergoes mainly elastic deformation, indicating the onset of elastoplastic behaviour. In the second regime, represented by $6 \le \frac{\delta_s}{\delta_{cs}} \le 110$, deformation is largely plastic, signifying a progression into a more advanced stage of elastoplastic deformation.

Also, the full elastic and plastic regime of a deformed asperity falls within the range of $0 \le \delta_s \le \delta_{cs}$, respectively $\delta_s \ge \delta_{cs}$.

These equations help us determine the dimensionless deformations and critical deformations of asperities in these specific regimes, aiding our understanding of the material behaviour during elastoplastic deformation.

Therefore, the full range of contact surfaces with fractal roughness behaviours for surfaces with fractal roughness with in the M.B. model [10, 23] can be reconfigured to include distinct regions: the completely elastic state, with $1 \le \frac{a_s}{a_{cs}} \le a_{ls}$, where a_{cs} represents dimensionless critical area, a_{ls} signifies the maximum area of actual contact between wheel and rail when an asperity undergoes deformation ($0 \le a_{ls} \le 1$), and this area is typically influenced by the shape and size of the asperities, as well as the applied forces and material properties. Following, appear initial elastoplastic stage $6^{1/(1-D)} \leq \frac{a_s}{a_{cs}} \leq 1$, subsequent elastoplastic phase, $110^{\frac{1}{1-D}} \leq \frac{a_s}{a_{cs}} \leq 6^{\frac{1}{1-D}}$ and final plastic stage, $0 \leq a_s \leq 110^{\frac{1}{1-D}} a_{cs}$.

The dimensionless contact loads In the first and second elastoplastic regimes (P_{sep1}, P_{sep2}) may be expressed by fractals depending on the roughness corresponding to the contact dimensionless area a_s follows:

$$P_{sep1}(a_s) = \frac{2a_2}{3a_1} kk_{HE} G_{fs}^{2(D-1)(b_2-b_1)} \bullet \left(\frac{2}{kk_{HE}}\right)^{2(b_2-b_1)} a_s^{(1-D)(b_2-b_1)+1}, P_{sep1} = \frac{P_{ep1}}{A_a E}. \quad (11)$$

$$P_{sep2}(a_s) = \frac{2a_{2p}}{3a_{1p}} kk_{HE} G_{fs}^{2(D-1)(b_2p-b_1p)} \left(\frac{2}{kk_{HE}}\right)^{2(b_2p-b_1p)} a_s^{(1-D)(b_2p-b_1p)+1}, \quad P_{sep2} = \frac{P_{ep2}}{A_a E}. \quad (12)$$

where P_{sep1} and P_{sep2}, denote the contact loads of a distorted asperity in the first and second elastoplastic regimes, and a_1, b_1, a_2, b_2, a_{1p}, b_{1p}, a_{2p} and b_{2p} are the constant [6], constants that are found in table no. 1.

Table 1

Value of constants for the various deformations of states [6].

First elastoplastic state	a_1	a_2	b_1	b_2
	0.93	1.03	1.136	1.425
Second elastoplastic state	a_{1p}	a_{2p}	b_{1p}	b_{2p}
	0.94	1.4	1.146	1.263

2.4 Plastic deformation regime

The full plastic regime of a deformed asperity falls within the range $\delta_s \geq \delta_{cs}$.

The dimensionless contact load in the plastic regime ($P_{sp}(a_s)$) could be written as follows:

$$P_{sp}(a_s) = k_{HE} a_s, P_{sp} = \frac{P_p}{A_a E}. \quad (13)$$

where P_p, with dimensionless form, P_{sp}, denote the contact loads of a distorted asperity in the plastic regime.

Finally, the dimensionless total contact load (P_{st}) is given by:

$$P_{st} = P_{se} + P_{sep1} + P_{sep2} + P_{sp}. \quad (14)$$

when $\delta_s \geq \delta_{cs}$, it follows that $a_s > a_{cs}$. This implies that if the contact area of a singular asperity exceeds the second critical elastoplastic contact zone, the asperity undergoes complete plastic deformation, with the relationship between load and area. These formulations capture the interplay between the contact area, the load on an asperity, and its interference across various conditions.

3. REAL CONTACT AREA

The real contact area depends on many factors, such as the wheel profile, rail profile, the vertical load on the wheel, and the modelled geometry.

The fractal nature of the contact surfaces between the locomotive wheel and the rail, determined through the roughness measurements of the rails at CTF Făurei and of the locomotive wheels at LEMA locomotive class 048, highlights a specific distribution of roughness, modelled by cosine waves, on the Hertzian elliptical contact surface. This configuration details how the asperities extend over the nominal surface, involving a complex and precise interaction between the wheel and the rail [24-25]. The distribution function of the contact spot $n(a)$ represents the distribution function of the contact spot area, which gives the probability that the contact spot size will be between a and $a+da$ and is provided by the formula in the dimensionless form:

$$n_s = nA_a, \quad n_s = \frac{D}{2}\left(\frac{a_{1s}^{D/2}}{a_s^{D/2+1}}\right)\Phi_e(D)^{\frac{2-D}{2}}, \quad (15)$$

Where, n represents the cumulative number of contact points on the nominal contact area (number of spots per mm²) with areas greater than a certain size threshold, denoted by area a_s, which depends on the normal load, and n_s is the dimensionless form of n. $\Phi_e(D)$ is the domain extension factor [22,26] associated with micro-contact size distribution, and it is linked to the fractal dimension (D) through the following formula:

$$\frac{\Phi_e^{\frac{2-D}{2}}-\left(1+\Phi_e^{\frac{-D}{2}}\right)^{\frac{D-2}{D}}}{\frac{(2-D)}{2}}=1. \quad (16)$$

Using the insights the preceding analysis provides, the real contact area A_r is derived from the cumulative contributions of the contact areas corresponding to the four distinct regimes. Therefore, it can be computed using the following equation for A_r with its dimensionless form A_{rs}:

$$A_r = A_e + A_{ep1} + A_{ep2} + A_p . \quad (17)$$

The following real area dimensionless are made:

$$A_{es}=\frac{A_e}{A_a}, A_{ep1s}=\frac{A_{ep1}}{A_a}, A_{ep2s}=\frac{A_{ep2}}{A_a},$$
$$A_{ps}=\frac{A_{ps}}{A_a}. \quad (18)$$

Thus, the contact area for each deformation state is given by:

$$A_{es}=\int_{a_{cs}}^{a_{1s}} a_s n_s da_s, A_{ep1s}=\int_{a_{cs2}}^{a_{cs}} a_s n_s da_s,$$
$$A_{ep2s}=\int_{a_{cs1}}^{a_{cs2}} a_s n_s da_s, A_{ps}=\int_{0}^{a_{cs1}} a_s n_s da_s. \quad (19)$$

In this context, A_e, A_{ep1}, A_{ep2} and A_p, respectively A_{es}, A_{ep1s}, A_{ep2s}, and A_{ps} represent the contact area and dimensionless contact areas associated with the four distinct regimes and a_l and its dimensionless form a_{ls} represent the maximum contact spot area, determined by the normal load.

Normal total load and its dimensionless forms could be elaborated upon as follows:

$$F_n = F_e + F_{ep1} + F_{ep2} + F_p . \quad (20)$$

Normal contact force for the four deformation states in the dimensionless form is given by:

$$F_{es}=\frac{F_e}{A_a E}, F_{ep1s}=\frac{F_{ep1}}{A_a E}, F_{ep2s}=\frac{F_{ep2}}{A_a E},$$

$$F_{ps}=\frac{F_{ps}}{A_a E}, F_{ns}=\frac{F_n}{A_a E}. \quad (21)$$

where F_{es}, F_{ep1s}, F_{ep2s}, *and* F_{ps} represent the contact loads corresponding to the four states, and F_{ns} is the dimensionless total contact load.

Finally, the contact normal load for each deformation state is given by:

$$F_{es}=\int_{a_{cs}}^{a_{1s}} P_{se} n_s da_s, F_{ep1s}=\int_{a_{cs2}}^{a_{cs}} P_{ep1s} n_s da_s,$$
$$F_{ep2s}=\int_{a_{cs1}}^{a_{cs2}} P_{ep2s} n_s da_s, F_{ps}=\int_{0}^{a_{cs1}} P_{ps} n_s da_s. \quad (22)$$

The equation gives the dimensionless total normal contact load for real contact area:

$$F_{nst}=F_{es}+F_{ep1s}+F_{ep2s}+F_{ps}. \quad (23)$$

This formulation captures the comprehensive impact of various contact regimes on the cumulative normal load, offering a refined understanding of the contact behaviour between simulated surfaces with fractal roughness.

4. TANGENTIAL CONTACT LOAD AND STATIC FRICTION COEFFICIENT

In the case of the friction analysis described above, the tangential load is the force that tries to initiate sliding or relative motion between wheel-rail contacting surfaces. Only the contacting asperities (microscopic surface irregularities) that undergo the fully elastic and the first elastoplastic regimes are able to support the tangential load [22-23, 27]. This means that only certain portions of the contacting surfaces, where the deformation remains within specific limits, can resist the force attempting to cause sliding. Furthermore, at the stage of sliding inception, the final yielding or plastic deformation occurs at the edge of the contact spot. This assumption is based on the distribution of the principal stresses within a deformed asperity at the interface [23,28-29]. This indicates that under the influence of the tangential load, the material experiences plastic flow, losing its ability to withstand further tangential loads without undergoing significant deformation.

The Tresca or von Mises criterion determines the onset of plastic deformation by asserting that yielding starts when the material's maximum shear stress reaches a specific threshold [20]. Utilising this criterion, the maximum dimensionless tangential load, T_{ts} (a_{ls}), can be deduced for surfaces with fractal roughness:

$$T_{ts} = \frac{8k_{yE}}{\pi(6-3\nu)}\left(A_{es} + A_{ep1s}\right) + \frac{8(2\nu-1)}{\pi(6-3\nu)}\left(F_{es} + F_{ep1s}\right),$$

$$k_{yE} = \frac{\sigma_y}{E}. \tag{24}$$

where k_{yE} represents the yield ratio with σ_y, yield stress. Then, the static friction coefficient $\mu_s(a_{ls})$ in the can be expressed as:

$$\mu_s(a_{ls}) = \frac{T_{tf}(a_{ls})}{F_{ns}(a_{ls})}. \tag{25}$$

Figures 2 and 3 depict the dependency of COF on F_{nst} (Eq. 23) and the fractal parameter D. To solve these dependencies was used the computer Matchad program.

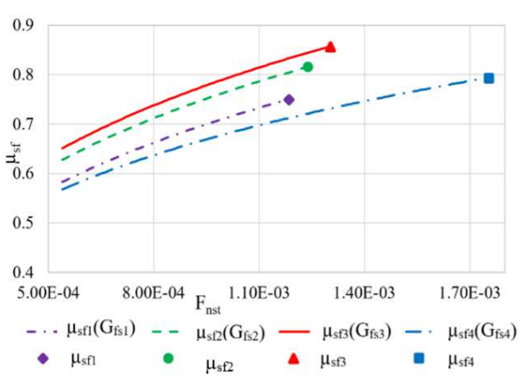

Fig. 2. Variation static friction coefficient (μ_{sf}) with contact load (F_{nst}).

The values of the fractal parameters defined by the roughness of the Faurei rail, the wheels of the LEMA locomotive class 048, and the wheel-rail samples from the UMT stand were determined using the Structure Function (SF) method [24,25]. Subsequently, equivalent fractal parameters were calculated to simplify the analysis of contact between the two rough surfaces by summing the rail and wheel structure functions. From these analyses, distinct sets of fractal parameters were obtained. The nominal areas (A_{a1}- A_{a4}) for the flat-cylinder material pairs, as well as for the wheel-rail pairs, were determined based on the Hertzian contact semi-axes of the wheel and the cylinder, the applied external forces, and the material properties of the specimens [30,31], the fractal parameters, G_{fs1}-G_{fs4}, were determined for each case, directly dependent on the nominal area. The values of the fractal parameters and the characteristics of the contact mechanics are presented in Table No. 2.

Table 2

Overview of Fractal Parameters and Contact Mechanics Characteristics

Parameter	Value
Equivalent fractal parameter D for laboratory wheel-rail	1.636
Equivalent fractal parameter D for wheel/rail	1.661
Equivalent scale parameter G_f for laboratory wheel-rail [mm]	$1.199 \cdot 10^{-7}$
Equivalent scale parameter G_f for wheel-rail [mm]	$1.389 \cdot 10^{-7}$
Dimensionless equivalent scale parameter G_{fs1} laboratory wheel-rail	$1.652 \cdot 10^{-7}$
Dimensionless equivalent scale parameter G_{fs2} laboratory wheel-rail	$1.389 \cdot 10^{-7}$
Dimensionless equivalent scale parameter G_{fs3} laboratory wheel-rail	$1.255 \cdot 10^{-7}$
Dimensionless equivalent scale parameter G_{fs4} for wheel-rail	$8.653 \cdot 10^{-6}$
Normal load (F_{n1}) cylinder plane contact [N]	20
Normal load (F_{n2}) cylinder plane contact [N]	40
Normal load (F_{n3}) cylinder plane contact [N]	60
Normal load (F_{n4}) for wheel-rail contact [N]	103.000
Nominal area A_{a1} for cilynder-plane under F_{n1} [mm^2]	0.528
Nominal area A_{a2} for cilynder-plane under F_{n2} [mm^2]	0.746
Nominal area A_{a3} for cylinder-plane contact under F_{n3} [mm^2]	0.914
Nominal area A_{a4} for wheel-rail contact under F_{n4} [mm^2]	208.7

In Figure 2, for wheel-rail laboratory pairs (μ_{sf1}, μ_{sf2}, *and* μ_{sf3}), the static friction coefficient (COF) increases with the dimensionless total normal load. This trend aligns with expectations since a greater normal force enhances the interlocking of surface asperities, thereby increasing friction.

Conversely, for the wheel-rail pair (μ_{sf4}), a lower static COF is observed even under significantly higher F_{nst}. So, this phenomenon can be attributed exclusively to the flow stress and hardness of the materials in the wheel-rail contact zone. Additionally, at very high normal forces, such as those in wheel-rail contact, asperities might be flattened or deformed more extensively, potentially leading to an apparently larger contact area but with less effective micro-level interlocking, resulting in a lower static COF. Nonetheless, the increasing trend suggests that even under these conditions, as the normal force continues to rise, the interactions between asperities and resistance to sliding begin to have a greater impact, leading to a gradual increase in the COF.

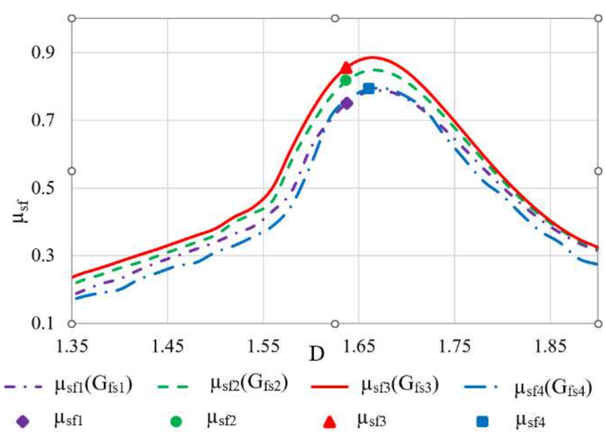

Fig 3. Variation static friction coefficient (μ_{sf}) with variable fractal parameter *D*.

From the example shown in Figure 3, it is observable that at low G_{fs} values, the static friction coefficient (COF) reaches its maximum and declines with an increase in G_{fs}, highlighting the significant influence of the scale factor on friction characteristics. Conversely, the static COF can be detected by *D* only within the range of 1.3-1.9. Outside this range, the absence of a discernible static COF could be due to specific surface interactions, deformation characteristics, or insufficient roughness engagement to produce measurable friction.

The COF is at its maximum for *D* in the range of 1.6-1.7 because this fractal dimension range corresponds to the most optimal balance between surface adherence and the elastic deformation capacity of the asperities. At these values, the asperities are sufficiently engaged to create resistance to sliding but are not so deformed that they allow easier sliding. Essentially, a *D* of approximately 1.6-1.7 may reflect a density and distribution of asperities that maximise the interaction and interlock between the contacting surfaces, thus leading to an increased COF.

For the wheel-rail pair, the COF value is the lowest shown in the graph, which can be explained by several factors specific to railway systems. Additionally, the wheels and rails in railway systems are subject to wear and smoothing processes during use, which can smooth out the asperities and reduce COF.

Moreover, due to the cyclic and repetitive nature of wheels passing over the same rail sections, a 'smooth' running path can form, further reducing the coefficient of friction compared to the laboratory-simulated conditions for wheel-rail contact.

5. DICUSSION AND CONCLUSION

Fractal modelling techniques were employed to theoretically evaluate the static friction coefficient within the context of Hertzian wheel-rail contact mechanics, accounting for surface roughness.

The fractal parameters *D* and G_{fs} directly impact the elastic regime, influencing the critical contact area (a_{cs}), critical deformation (δ_{cs}), and the elastic contact force P_{se}.

The transition from the elastic to the elastoplastic regime (first and second) is aptly captured by the fractal parameters *D* and G_{fs}, which affect the surface roughness and asperity interactions, impacting the contact loads P_{sep1} and P_{sep2} and exerting a direct influence on the critical areas (a_{cs1}, a_{cs2}), critical deformations (δ_{cs1}, δ_{cs2}).

When a material achieves its fully plastic state, asperities undergo substantial deformation, diminishing the relevance of initial surface characteristics and fractal parameters like *D* and G_{fs}. The initial surface roughness and fractal characteristics become secondary as material properties dominate, causing fractal parameters like D and G_{fs} to lose their significance in describing contact behaviour.

In the context of total contact load, P_{st}, variations in fractal parameters D and G_{fs} significantly influence the elastic and elastoplastic regimes but have no discernible impact on the full plastic regime.

In Hertzian wheel-rail contact, the fractal parameter D influences the real contact area (A_{rs}) and the largest spot size (a_{ls}), indirectly affecting acoustic emissions and noise generation.

Despite variations in asperity density with G_{fs} changes, the size of the largest asperities predominantly influences the real contact area, and G_{fs} shows no direct impact on the real contact area.

The total normal load, F_{nst}, interacts with the fractal parameter D, especially in the range 1.4-1.8. With the maximum spot area reduction, parameter D extends its applicability to its maximum capacity. The surface characteristics largely corroborate the behaviour of F_{nst}, the fractal dimensions, and the forces applied, and they emphasise the complex balance of these determinants in the governance of contact mechanics.

The static COF is intricately influenced by factors such as maximum spot area a_{ls}, the scale factor G_{fs}, applied force, and the fractal parameter D. Their interplay dictates the frictional behaviour, underscoring the importance of understanding these parameters when evaluating surface interactions.

6. REFERENCES

[1] Demkin N. B., Izmailov V. V., *Surface Topography and Properties of Frictional Contacts*, Tribology International, 1991, 24(1): 21 - 24.

[2] Popov L. V., *Contact Mechanics and Friction*, Physical Principles and Applications, Springer, 2009.

[3] Persson Bo. N. J., Tossati E., *Physics of sliding friction*, 1995, Series E, Applied Science, 311.

[4] Chang W.R., Etsion I., Bogy David. B., *Static friction coefficient model for metallic rough surfaces*, ASME J. Tribol., 1988, 110, 57 - 63.

[5] Zhao Y. W., Maietta D. M., L. Chang, *An asperity micro-contact model incorporating the transition from elastic deformation to fully plastic flow*, ASME J. Tribol., 2000, 122, 86 - 93.

[6] Kogut L., Etsion I., *Elastic–plastic contact analysis of a sphere and a rigid flat*, ASME J. Appl. Mech., 2002, 69, 657 - 662.

[7] J. A. Greenwood, PhD, and J. H. Tripp, *The Contact of Two Nominally Flat Rough Surfaces*, Proc. Inst. Mech. Eng.,185(1), 1970, 625 – 633.

[8] Dowson D., *History of tribology. 2nd ed. London:* Professional Engineering Publishers, 1998.

[9] Majumdar A. and Bhushan B., *Role of fractal geometry in roughness characterisation and contact mechanics of surfaces*, J. Tribol., 112, 1990, 205 - 216.

[10] Majumdar A., Bhushan B., *Fractal model of elastic–plastic contact between rough surfaces*, ASME J. Tribol., 1991, 113, 1 - 11.

[11] Chang W. R., Etsion I., Bogy B. D., *An elastic-plastic model for the contact of rough surfaces*, ASME J. Tribol., 1987, 109, 257 - 263.

[12] Kogut L., Etsion I., *A semi-analytical solution for the sliding inception of a spherical contact*, ASME J. Tribol., 2003, 125, 499 - 506.

[13] Kogut L., Etsion I., *A static friction model for elastic-plastic contacting rough surfaces*, ASME J. Tribol., 2004, 126, 34 - 40.

[14] Sheng X., Luo J., Wen S., *Static Friction Coefficient Model Based on Fractal Contact* [J]. China Mechanical Engineering, 1998, (7), 16 - 18.

[15] Tian H., Zhao C., Fang Z., Zhu D.L., Chen B. and Li X., *Predication investigation on static tribological performance of metallic material surfaces-theoretical model*, Journal of Vibration and Shock, 2013 - 1, 32 (12): 40 - 44, 66.

[16] Tian H., Zhu D., Qin H., *Fractal model of static friction coefficient of joint interface and its simulation*, Chinese Journal of Applied Mechanics, 2011, 28(2): 158 - 162.

[17] Zhang Y., Zhang X., Jiang L., et al. *Fractal Model of Static Frictional Coefficient on Joint Surface Considering Elastic-plastic*

Deformation, Journal of Taiyuan University of Science and Technology of China, 2014, 25(4): 294 - 301.

[18] Yuan Y., Gan L., Liu K., & Yang X., 2016. *Elastoplastic contact mechanics model of rough surface based on fractal theory*, Chinese Journal of Mechanical Engineering, 30(1), 207 - 215.

[19] Morag Y., Etsion I., *Resolving the contradiction of asperities plastic to elastic mode transition in current contact models of fractal rough surfaces* [J]., Wear, 2007, 262(5), 624 - 629.

[20] Johnson K. L., *Contact mechanics* [M]. Cambridge: Cambridge University Press, 1987.

[21] Li L., Wang J., Shi X., Ma S., and Cai A., *Contact stiffness model of joint surface considering continuous smooth characteristics and asperity interaction*, Tribology Letters, 2021, 69(2): 1 - 12.

[22] Zhang C., LI X., He J.L., Cheng Y.H., Liu Z., and Li Y., *Static friction coefficient model of joint surface based on the modified fractal model and experimental investigation*, The International Journal of Advanced Manufacturing Technology, 2022**,** 124 (11-12), 1-15.

[23] J-M You and T-N Chen*, A static friction model for the contact of fractal surfaces,* Proc. IMechE Vol. 224 Part J: J. Engineering Tribology, 2010, 513-518.

[24] Babici L. M., Tudor A., J. Romeu, M. Stoica, *Fractal evaluation aspects in characterising the roughness of a driving wheel from a locomotive*, Institute of Physics (IOP), IOP Conference Series: Materials Science and Engineering, 01/01/2020, 724, 1, 1757-8981.

[25] Babici L. M., Tudor A., *Some aspects regarding the roughness of the railway surface and rolling noise at locomotives*, Institute of Physics (IOP), IOP conference series: materials science and engineering, 26/06/2019, 514, 012010:1 - 012010:14, 1757-899X.

[26] Wang S., Komvopoulos K., *A fractal theory of the temperature distribution at elastic contacts of fast sliding surfaces*, ASME J. Tribol., 1995, 117, 203 - 214.

[27] Kogut L., Etsion I., *A semi-analytical solution for the sliding inception of a spherical contact*, ASME J. Tribol., 2003, 125, 499 - 506.

[28] Kogut L., Etsion I., *A static friction model for elastic-plastic contacting rough surfaces*, ASME J. Tribol., 2004, 126, 34 - 40.

[29] Zhao B., Xu H. & Lu X., 2019. *Sliding Interaction for Coated Asperity with Power-Law Hardening Elastic-Plastic Coatings*, Materials, 12(15), 2388.

[30] Esveld C, Modern Railway Track, MRT Productions, 2001, Chap 2.

[31] Thompson D. J., Railway Noise and Vibration: Mechanisms, Modelling and Means of Control. Elsevier Ltd, 2009.

Modelarea fractală a Coeficientului de Frecare Statică în Contactul Hertzian Eliptic pentru roata sina

În cadrul acestui studiu, s-a determinăm coeficientul de frecare statică prin utilizarea unei abordări fractale, care combină principiile fundamentale ale geometriei fractale cu mecanica contactului atât în sistemele roată-șină Hertziană cât și în interacțiunile epruvetelor-cilindru plan care implică suprafețe cu rugozitati. Utilizând modelul Weierstrass-Mandelbrot, studiul examinează tranziția prin diferite stări de deformare, considerând COF static ca fiind un indicator al proprietăților intrinseci ale materialului mai moale și influențat de parametrii fractali. În contrast cu ipoteza tradițională a unei suprafețe de contact omogene, acest studiu integrează proprietățile fractale pentru a calcula mai precis suprafața de contact reală. Această abordare oferă o înțelegere mai nuanțată a interacțiunilor de suprafață, stabilind COF static ca factor crucial pentru aderență și indicator de performanță în operațiunile feroviare.

Laura Mariana BABICI, dr. eng. Romanian Railway Authority, Bucharest, Romania, lbabici@yahoo.com

Andrei TUDOR, prof. Dr. Department of Machine Elements and Tribology, National University of Science and Technology Politehnica Bucharest, 313 Splaiul Independentei, 060042, Romania, andreitudor1947@gmail.com.

Jordi ROMEU, prof. Dr. Acoustical and Mechanical Engineering Laboratory (LEAM), Universitat Politècnica de Catalunya (UPC), c/Colom, 11, 08222 Terrassa, Spain, jordi.romeu@upc.edu.